PHYSICAL REVIEW B **76**, 020404(R) (2007)

Impurity conduction and magnetic polarons in antiferromagnetic oxides

C. Chiorescu and J. L. Cohn
Department of Physics, University of Miami, Coral Gables, Florida 33124, USA

J. J. Neumeier
Department of Physics, Montana State University, Bozeman, Montana 59717, USA

(Received 5 July 2007; published 27 July 2007)

Low-temperature transport and magnetization measurements, reported for the antiferromagnets $SrMnO_3$ and $CaMnO_3$, provide a means for distinguishing self-trapped from bound magnetic polaron (MPs) and reveal new insight into the role of impurity states on MP formation in oxides. The data identify an impurity band of mobile states separated by energy δ from electrons bound in Coulombic potentials. Very weak electric fields are sufficient to excite bound electrons to the impurity band, increasing the mobile carrier concentration by more than three orders of magnitude. The data indicate that *bound* MPs become stable only for $k_BT \ll \delta$.

DOI: 10.1103/PhysRevB.76.020404 PACS number(s): 75.47.Lx, 71.27.+a, 71.55.−i, 72.20.−i

An electron in a magnetic solid can perturb local moments via exchange interactions between its spin and those of the ions, forming a self-trapped or bound magnetic polaron (MP). Though these concepts were formulated long ago,[1] experimental understanding and theoretical development of MP physics have been limited by the relatively small number of materials found to manifest MPs. More recently, renewed interest in the MP problem has been stimulated by studies of carrier-doped antiferromagnetic (AF) manganites[2] and dilute magnetic semiconducting oxides.[3] An important emerging issue for both classes of compounds is the energy position of donor levels (e.g., associated with oxygen vacancies and/or impurities) within the band gap and the contribution of donor-bound charge to MP formation.

Perhaps the simplest AF systems for examining such issues are the nominally Mn^{4+} compounds, $CaMnO_3$ (CMO) and $SrMnO_3$ (SMO), which have a bipartite (*G*-type) AF ground state and are free from the complex collective interactions of Jahn-Teller-active Mn^{3+} ions that characterize more widely studied $LaMnO_3$. They are model systems for MP studies since the couplings between electronic, lattice, and spin degrees of freedom for light electron doping are known.[4,5] Magnetization[6] and scattering[7] studies imply the existence of MPs in the ground state of CMO when electron doped with La, and theory[4,5] predicts these electrons form self-trapped MPs, i.e., those bound solely by magnetic exchange interactions with ionic spins. A reliable means of experimentally distinguishing self-trapped from bound MPs (electrons bound in Coulombic potentials that polarize surrounding spins) is not established. While an activated conductivity is expected for bound MPs, theory predicts[5] self-trapped MPs to exhibit either metallic or activated behavior depending on the strength of magnetic coupling. Furthermore, shallow impurity states associated with oxygen vacancies are ubiquitous in oxides, and their influence on the energetics of MP formation and their transport has not been addressed theoretically or experimentally.

Here we report low-temperature transport and magnetic studies on CMO and SMO, which offer new insight into the role of impurity states on MP formation and provide a means of distinguishing self-trapped from bound MPs. This distinction is made possible by a favorable electronic structure, consisting of an impurity band of mobile electronic states positioned at a small energy δ ($\sim$3.5 meV for SMO) above those of electrons bound in Coulombic potentials (bound MPs). Very weak electric fields ($F \leqslant 50$ V/cm) are sufficient to excite these electrons to the impurity band, increasing the mobile carrier concentration by more than three orders of magnitude. For the present compounds, bound MPs become stable only for $k_BT \ll \delta$. A similar energy-level scheme may be expected in other oxides, and thus the tunable mobile carrier density reported here could be further exploited for novel studies of correlated electrons.

The synthesis procedures for the single crystal of $CaMnO_3$ (CMO) and the polycrystalline specimen of $SrMnO_3$ (SMO) are described elsewhere.[6,8–10] The net electron densities determined from Hall measurements at room temperature were $n_H \equiv N_D - N_A \simeq 6 \times 10^{18}$ cm^{-3} (CMO) and 3×10^{18} cm^{-3} (SMO). These correspond to $\approx 10^{-3} - 10^{-4}$ electrons per formula unit, attributable to a very small oxygen deficiency. Compensating impurities (e.g., from ppm levels in the starting chemicals) are typical in oxides; the $T = 300$ K thermopowers[11] of $-420\ \mu$V/K (CMO) and $-180\ \mu$V/K indicate a greater compensation in SMO. The dc resistivity and Hall coefficient were measured in a 9 T magnet on six-probe specimens with silver paint contacts. Magnetic field was applied perpendicular to the plane of platelike specimens in which dc currents (5 nA–10 mA) were applied. Both current and field reversal were employed for Hall and magnetoresistance measurements. A thermocouple attached to each specimen monitored temperature rises due to self-heating, observed only at the highest currents employed. Magnetization measurements were performed in a Quantum Design PPMS.

CMO and SMO are orthorhombic and cubic, respectively, with[12] $T_N \simeq 125$ and[8] 230 K. They are weakly ferromagnetic (FM) at low T, with saturation magnetizations $\sim 0.02 - 0.03 \mu_B$/Mn ion,[6,8] but the FM moment develops abruptly at $T < T_N$ for CMO and gradually[8] at $T \lesssim 80$ K $\ll T_N$ for SMO (Fig. 1, inset). The latter behavior appears to be associated with FM polarons,[7] whereas the former may be attributed to an additional FM contribution in CMO from Dzyaloshinsky-Moriya coupling (allowed by symmetry). Assuming isolated

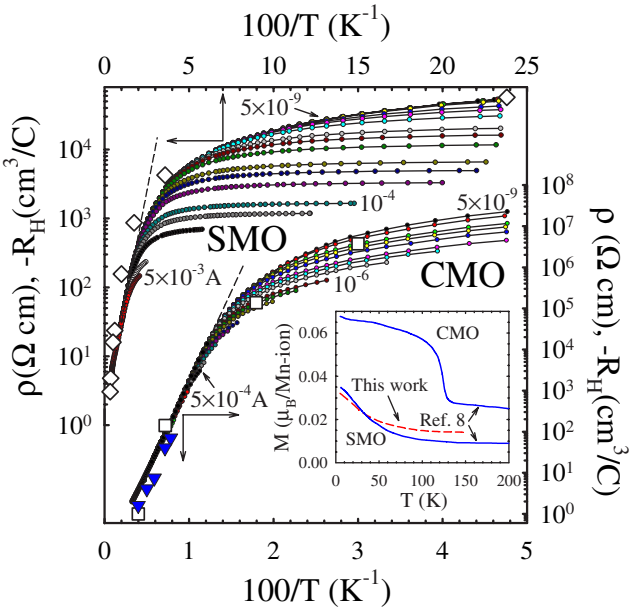

FIG. 1. (Color online) ρ vs $100/T$ for SMO (upper abscissa, left ordinate) and CMO (lower abscissa, right ordinate). Each curve was measured with a different dc current, some of which are labeled; increases are in steps of 1, 3, 5 per decade. Dashed lines are linear fits. Hall coefficients (open squares and diamonds) were measured at the lowest currents. Inverted triangles are Hall data for polycrystalline CMO from Ref. 9. Inset: $M(T)$ at $H=50$ kOe for SMO and CMO.

MPs, the ratio of the saturation magnetization and electron density implies that each doped electron produces a moment of $\sim(50-100)\mu_B$, corresponding to the polarization of $\sim(30-70)$ Mn^{3+} spins. For a spherical volume, this yields a MP radius $\sim(7-11)$ Å.

Figure 1 shows resistivity data (in zero magnetic field), plotted versus inverse temperature, illustrating the sensitivity of the charge transport in these materials to applied current (I) at low T where impurity conduction is predominant. Several curves for each specimen are labeled by values of I; successive curves represent current increases in steps of 1, 3, and 5 per decade.

The high-T resistivity has an activated form, $\rho \propto \exp(\Delta/k_BT)$, with $\Delta=86$ meV and 25 meV for CMO and SMO, respectively (dashed lines, Fig. 1). The Hall coefficients (R_H) measured at the lowest currents (open squares and diamonds, Fig. 1) follow $\rho(T)$ in their temperature variation, consistent with thermal activation of electrons from donor levels[13] to the conduction band and a weakly T-dependent mobility. Both ρ and R_H become weakly T dependent in the impurity conduction regime at the lowest T, indicating that only a small fraction of bound carriers are sufficiently mobile at low T to contribute to R_H.

Isothermal measurements of conductivity (σ) vs applied current density (J) indicate that in the non-Ohmic regime σ scales with the transport electric field ($F \equiv \rho J$) as, $\sigma(F)/\sigma_0 \propto \exp(\alpha\sqrt{F})$, where $\sigma_0 \equiv \sigma(I=5$ nA). This is shown for SMO in Fig. 2(a). The temperature dependence of the parameter α, determined from least-squares fits [solid lines, Fig. 2(a)], is

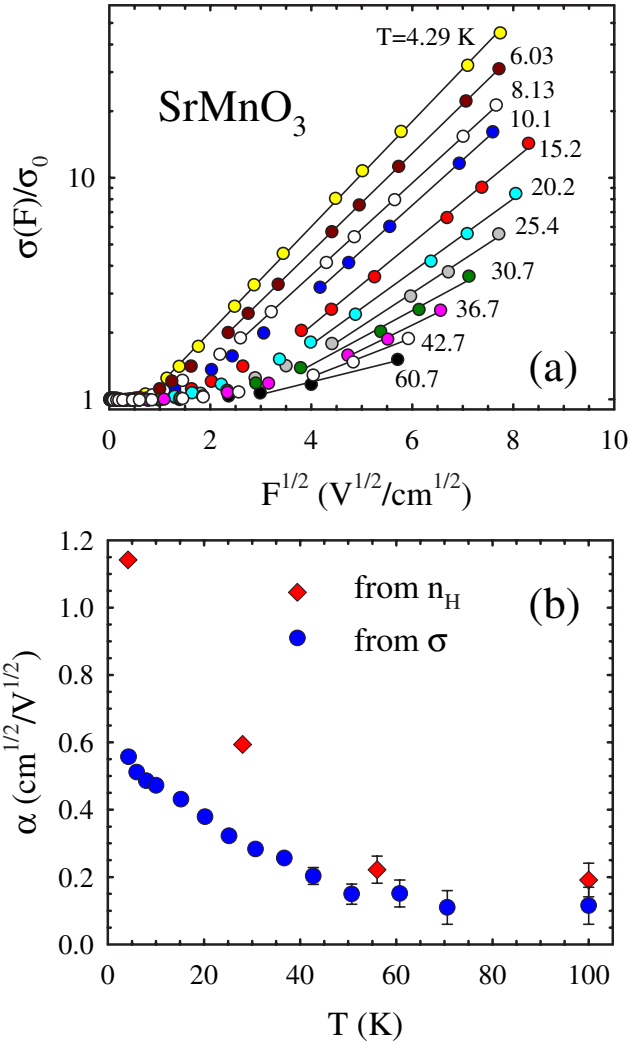

FIG. 2. (Color online) (a) Semilogarithmic plot of $\sigma(F)/\sigma_0$ vs $F^{1/2}$ for SMO at various temperatures. Solid lines are linear fits. (b) Slopes α, determined from (a) (solid circles) and from a similar analysis of the Hall density (Fig. 4).

plotted in Fig. 2(b). This dependence of σ on F is that prescribed by Poole-Frenkel field-assisted ionization[14,15] of carriers bound to donors, and is discussed in more detail below. Note that α was found to be independent of applied magnetic field up to 9 T in spite of a modest magnetoresistivity, e.g., $\Delta\rho/\rho|_{9T} \simeq -0.13$ and -0.04 for $I=5$ nA and 0.5 mA, respectively, at $T=28$ K for SMO. Heating of the sample can be ruled out as the cause of the F dependence because specimen temperature was monitored directly with a thermocouple, was limited to $\lesssim 2-3$ K at the highest current for each temperature, and was corrected for by interpolation on the $\rho(T)$ curves at fixed I. Qualitatively similar results have been observed for these same specimens after annealing to vary their oxygen content, and for polycrystalline CMO and $Ca_{0.25}Sr_{0.75}MnO_3$.[11]

The current and magnetic field dependencies of the Hall resistivity, ρ_{xy} (Fig. 3), provide further evidence that Poole-Frenkel ionization of trapped carriers underlies the non-Ohmic behavior of σ. This plot shows ρ_{xy} vs magnetic field

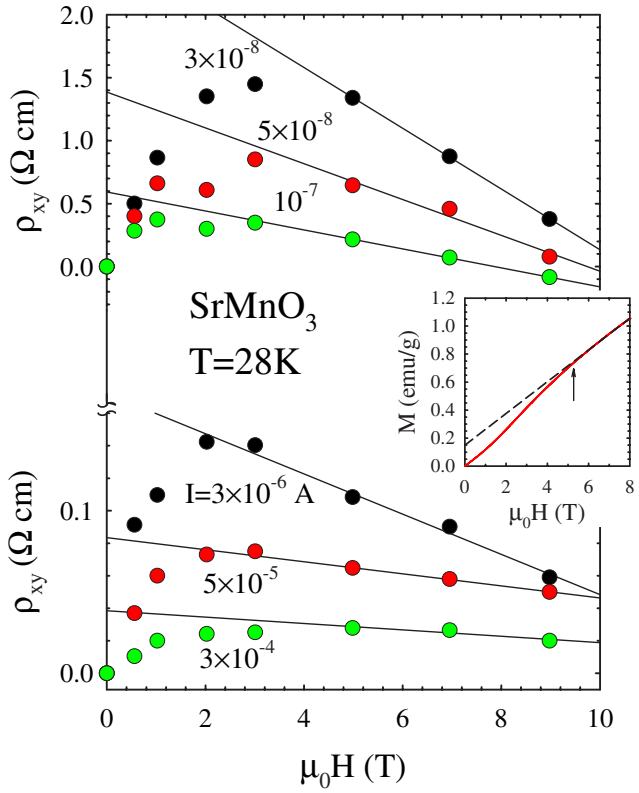

FIG. 3. (Color online) Hall resistivity vs magnetic field for SMO at $T=28$ K. Different curves are labeled by the applied current. The solid lines are linear fits at the highest fields used to determine the normal Hall contribution. The inset shows the magnetization at the same temperature (solid curve) and linear fit to the high-field data (dashed line).

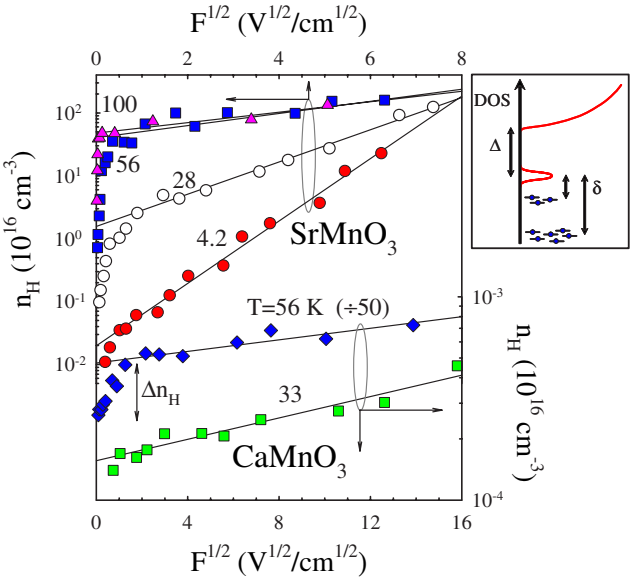

FIG. 4. (Color online) Semilogarithmic plots of Hall carrier density vs $F^{1/2}$ at different temperatures for CMO (lower abscissa, right ordinate) and SMO (upper abscissa, left ordinate). Solid lines are linear fits. Inset: energy-band scheme implied by the temperature and electric-field dependence of n_H (see text).

for SMO at $T=28$ K for several values of the applied current. With increasing field, ρ_{xy} for each current increases to a maximum near $\mu_0 H \sim 3$ T, and becomes linear in field for $\mu_0 H \gtrsim 5$ T. This behavior indicates a sum of (positive) anomalous and (negative) normal Hall contributions, consistent with the magnetization (inset, Fig. 3), which exhibits a small FM contribution superposed with the linear AF background. The FM component saturates for $\mu_0 H \gtrsim 5$ T, and the magnetization becomes linear in field (dashed line) in the same field range as does ρ_{xy}. The normal Hall coefficient was determined from the high-field slopes, $R_H = d\rho_{xy}/d(\mu_0 H)$ (solid lines, Fig. 3). Both R_H and the anomalous contribution to ρ_{xy} (intercept of solid lines) decrease systematically with increasing current, signaling an increase in the mobile carrier density.

Figure 4 shows the Hall carrier density $n_H \equiv 1/(R_H e)$, plotted vs $F^{1/2}$ for CMO (lower abscissa, right ordinate) and for SMO (upper abscissa, left ordinate) at several temperatures. The ionization rate in the Poole-Frenkel model[14,15] incorporates thermal activation as well as field-induced barrier lowering. At low T, where the majority of electrons are trapped, the Hall density should be of the form $n_H(F) \approx N^0 \exp[-(\delta/k_B T - \alpha\sqrt{F})]$, where N^0 is the density of neutral donors and δ is the barrier height. The scale for barrier lowering is set by $\alpha = \beta/k_B T$, where $\beta = (Ze^3/\pi\epsilon_0\epsilon_r)^{3/2}$ and ϵ_r is an effective relative dielectric constant, often taken to be the high-frequency (optical) value. The low-T values of α determined from the slopes of linear least-squares fits (solid lines, Fig. 4) imply $\beta \simeq 0.2$ meV cm$^{1/2}$/V$^{1/2}$ (CMO) and 0.4 meV cm$^{1/2}$/V$^{1/2}$ (SMO), in reasonable accord with the value 0.34 meV cm$^{1/2}$/V$^{1/2}$ (0.48 meV cm$^{1/2}$/V$^{1/2}$) estimated for manganites using $Z=2$ ($Z=1$), for singly (doubly) occupied vacancies, and[16] $\epsilon_r \simeq 5$.

A compelling feature of the $n_H(F)$ data is that at each temperature, n_H extrapolates toward the value $n_H(300\ \mathrm{K})$, the latter presumably reflecting nearly full ionization of donors to the conduction band. This implies that *all* carriers are bound in Coulomb potentials in the ground state, and thus rules out the existence of self-trapped magnetic polarons. A much weaker field effect in $n_H(F)$ for CMO is consistent with the smaller influence of F on the resistivity (Fig. 1). The difference in the magnitude of the field effect for the two compounds implies a difference in the potential barrier for donor ionization δ. Applying the expression for n_H above to the low-T n_H data, with $N^0 = N_D - N_A \approx n_H(300\ \mathrm{K})$, yields $\delta \simeq 41$ and 3.5 meV for CMO and SMO, respectively. We conclude that electrons are not ionized to the conduction band (requiring energy $\sim\Delta$), but are rather excited to a band of more mobile impurity states responsible for the low-T conduction, as depicted in the inset of Fig. 4.

Differing local environments, e.g., associated with vacancy clusters or vacancy-acceptor pairs,[17] are expected to result in multiple bound-state energies. With increasing T electrons with larger binding energies are promoted to the impurity band and rendered mobile in applied field F so that the $n_H(F,T)$ data provide for impurity-level spectroscopy. The $n_H(F)$ curves for SMO at 28, 56, and 100 K imply $\delta \approx 14 \pm 3$ meV, indicating that there are principally two such bound-state energies (inset, Fig. 4).

Two aspects of the data indicate a strong electric-field dependence of the Hall mobility. A low-field increase in the carrier density, designated Δn_H in Fig. 4 (vertical arrows), comes to predominate in the total field effect as T increases. We attribute it to carriers thermally excited to the impurity band where they are more loosely bound and mobile at low fields. This field regime corresponds to *Ohmic* behavior in σ (Fig. 2), and thus implies $\mu_H \propto n_H^{-1}$. At higher fields within the Poole-Frenkel ionization regime, the values of α for SMO determined from $\sigma(F)$ are substantially lower than those determined from $n_H(F)$ [Fig. 2(b)], by an amount that grows with decreasing T at $T \lesssim 60\ \mathrm{K} \approx \delta$. At 4.2 K, $\alpha_{n_H} \approx 2\alpha_\sigma$, implying $\mu_H \propto n_H^{-1/2}$. These observations suggest interesting correlation effects within the impurity band. It is plausible that MP detrapping in the electric field locally depolarizes a number of Mn spins. The impurity-band carrier mobility may thus be influenced by changes in both magnetic and Coulomb interactions associated with detrapping.

It is likely that transport in the impurity band involves next-nearest-neighbor Mn e_g orbitals given that nearest-neighbor hopping in the G-type AF lattice is strongly inhibited by Hund's rule. This band may involve excited impurity states since little overlap is to be expected between bound states with a mean spacing, $\approx 2[3/4\pi(N_D - N_A)]^{1/3} \sim 60 - 80$ Å, and radius $\sim 7 - 11$ Å (estimated above).

That the FM contribution to the magnetization in SMO develops only below ~ 80 K (Fig. 1, inset) implies that bound MPs become stable only for $k_B T \ll \delta$. The material parameters which control δ are thus of particular interest for the physics of MP formation. The larger values of Δ and δ for CMO suggest an intrinsic origin (e.g., the buckled Mn-O-Mn bond), but compensation may also play a role, and further studies are called for to address this issue.

In summary, the results reported here for G-type antiferromagnetic oxides reveal an intriguing interplay between defect states and MP formation. A distinction between self-trapped and bound MPs is made possible by the presence of a mobile band of impurity states to which electrons, bound at energy δ below, are excited through barrier lowering in weak electric fields. Such an impurity band, derived from states involving oxygen vacancies, is likely common to other oxides where similar features in the transport might be observed. Such measurements can be employed as a tool for impurity-level spectroscopy and for studying correlated electrons with a tunable mobile carrier density.

The authors acknowledge helpful comments from S. Satpathy. This material is based upon work supported by the National Science Foundation under Grants No. DMR-0072276 (University of Miami) and No. DMR-0504769 (Montana State University), and the Research Corporation (University of Miami).

[1] E. L. Nagaev, Zh. Eksp. Teor. Fiz. Pis'ma Red. **6**, 484 (1967) , [JETP Lett. **6**, 18 (1967)]; T. Kasuya, A. Yanase, and T. Takeda, Solid State Commun. **8**, 1543 (1970); A. Mauger and D. L. Mills, Phys. Rev. B **31**, 8024 (1985); L. Liu, Phys. Rev. B **37**, 5387 (1988).

[2] See, e. g., *Colossal Magnetoresistance, Charge Ordering and Related Properties of Manganese Oxides*, edited by C. N. R. Rao and B. Raveau (World Scientific, Singapore, 1998); E. Dagotto, *Nanoscale Phase Separation and Colossal Magneto-resistance, Springer Series in Solid-State Sciences* Vol. 136 (Springer-Verlag, Berlin, 2003).

[3] C. Liu, F. Yun, and H. Morkoç, J. Mater. Sci.: Mater. Electron. **16**, 555 (2005); J. M. D. Coey, M. Venkatesan, and C. B. Fitzgerald, Nat. Mater. **4**, 173 (2005); K. R. Kittilstved, D. A. Schwartz, A. C. Tuan, S. M. Heald, S. A. Chambers, and D. R. Gamelin, Phys. Rev. Lett. **97**, 037203 (2006).

[4] Y.-R. Chen and P. B. Allen, Phys. Rev. B **64**, 064401 (2001).

[5] H. Meskine, T. Saha-Dasgupta, and S. Satpathy, Phys. Rev. Lett. **92**, 056401 (2004); H. Meskine and S. Satpathy, J. Phys.: Condens. Matter **17**, 1889 (2005).

[6] J. J. Neumeier and J. L. Cohn, Phys. Rev. B **61**, 14319 (2000).

[7] E. Granado, C. D. Ling, J. J. Neumeier, J. W. Lynn, and D. N. Argyriou, Phys. Rev. B **68**, 134440 (2003).

[8] O. Chmaissem, B. Dabrowski, S. Kolesnik, J. Mais, D. E. Brown, R. Kruk, P. Prior, B. Pyles, and J. D. Jorgensen, Phys. Rev. B **64**, 134412 (2001).

[9] J. L. Cohn, C. Chiorescu, and J. J. Neumeier, Phys. Rev. B **72**, 024422 (2005).

[10] J. L. Cohn, M. Peterca, and J. J. Neumeier, Phys. Rev. B **70**, 214433 (2004).

[11] C. Chiorescu, J. L. Cohn, and J. J. Neumeier (unpublished).

[12] E. O. Wollan and W. C. Koehler, Phys. Rev. **100**, 545 (1955).

[13] The calculated band gaps are ~ 0.4 and 0.3 eV for CMO and SMO, respectively. See, e.g., W. E. Pickett and D. J. Singh, Phys. Rev. B **53**, 1146 (1996); R. Søndenå, P. Ravindran, S. Stølen, T. Grande, and M. Hanfland, *ibid.* **74**, 144102 (2006).

[14] J. Frenkel, Phys. Rev. **54**, 647 (1938).

[15] J. G. Simmons, Phys. Rev. **155**, 657 (1967); J. L. Hartke, J. Appl. Phys. **39**, 4871 (1968); J. R. Yeargan and H. L. Taylor, *ibid.* **39**, 5600 (1968); G. A. Dussel and K. W. Boer, Phys. Status Solidi **39**, 375 (1970).

[16] A. S. Alexandrov and A. M. Bratkovsky, J. Phys.: Condens. Matter **11**, L531 (1999).

[17] B. I. Shklovskii and A. L. Efros, *Electronic Properties of Doped Semiconductors* (Springer-Verlag, New York, 1984).